



CHORUS

This is the accepted manuscript made available via CHORUS. The article has been published as:

## Percolation Model of Sensory Transmission and Loss of Consciousness Under General Anesthesia

David W. Zhou, David D. Mowrey, Pei Tang, and Yan Xu

Phys. Rev. Lett. **115**, 108103 — Published 4 September 2015

DOI: [10.1103/PhysRevLett.115.108103](https://doi.org/10.1103/PhysRevLett.115.108103)

**A Percolation Model of Sensory Transmission and  
Loss of Consciousness under General Anesthesia**

David W. Zhou<sup>1,5,&</sup>, David D. Mowrey<sup>1,2,&</sup>, Pei Tang<sup>1,2,3</sup>, and Yan Xu<sup>1,3,4,\*</sup>

Departments of <sup>1</sup>Anesthesiology, <sup>2</sup>Computational and Systems Biology, <sup>3</sup>Pharmacology & Chemical Biology, and <sup>4</sup>Structural Biology, University of Pittsburgh School of Medicine; and <sup>5</sup>Department of Biological Sciences, Carnegie Mellon University, Pittsburgh, PA

<sup>&</sup>Authors with equal contributions

\*Address all correspondence to:

Professor Yan Xu, PhD

2048 Biomedical Science Tower 3

University of Pittsburgh School of Medicine

3501 Fifth Avenue

Pittsburgh, PA 15213

Telephone: (412) 648-9922

Fax: (412) 648-8998

Email: [xuy@anes.upmc.edu](mailto:xuy@anes.upmc.edu)

**Running title:** Percolation model of sensory transmission

## **Abstract**

Neurons communicate with each other dynamically. How such communications lead to consciousness remains unclear. Here, we present a theoretical model to understand the dynamic nature of sensory activity and information integration in a hierarchical network, in which edges are stochastically defined by a single parameter,  $p$ , representing percolation probability of information transmission. We validate the model by comparing the transmitted and original signal distributions and show that a basic version of this model can reproduce key spectral features clinically observed in electroencephalographic recordings of transitions from conscious to unconscious brain activities during general anesthesia. As  $p$  decreases, a steep divergence of the transmitted signal from the original was observed, along with a loss of signal synchrony and a sharp increase in information entropy in a critical manner, resembling the precipitous loss of consciousness during anesthesia. The model offers mechanistic insights into the emergence of information integration from a stochastic process, laying the foundation to understand the origin of cognition.

**Keywords:** cognition; electroencephalograph (EEG); general anesthesia; loss of consciousness; neural network; thalamocortical and cortico-cortical synchrony

Structural and functional neuroimaging studies have mapped the connectivity of neuroanatomy and networks at ever-increasing resolution [1-5]. Analyses assigning cognitive roles to structural or functional regions demonstrate mechanism based on functionalism and not on neurobiological first principles, failing to bridge matter and mind [6]. In most analyses, cognition is claimed to arise in a large-scale functional network exhibiting co-activation of brain regions during a given task [4]. Although this definition of cognition usefully relates structure to function [4], its theoretical framework is circular and offers limited value in understanding basic principles governing the emergence of cognition.

Circumventing this theoretical gap, several studies modeled individual electroencephalographic (EEG) features associated with loss of consciousness during general anesthesia [7-14]. Dynamic causal modeling was used to describe EEG spectral power under anesthesia-induced unconsciousness [15]. Metabolism dynamics was used to account for burst suppression [12]. A stochastic model was developed to describe general anesthesia as a thermodynamic phase transition [7,8]. A more detailed account of anesthetic effects on ion channels was used to parameterize a mean-field theory of electrocortical activities [16]. An information integration theory [17] treated consciousness as a unified state in a complex system that gains quantifiable information as a whole relative to the parts. An empirical measure was recently developed to assess information integration under different conscious states [18]. However, few theoretical advances explain multiple EEG features while accounting for information flow and integration *ab initio* without making causal assumptions of the system. A systems-level theory is needed to explain sensory processing under deep anesthesia [19]. No existing model accounts for EEG features under anesthesia, disruption of information flow, and neurobiological function together.

Here, we applied neurobiological first principles to information transmission in a neural network constructed based on the thalamocortical and corticocortical topology. We used percolation theory to calculate information access between nodes. The model reveals coherence emergence at a critical threshold by varying only one parameter governing probability with which an edge is connected. It generates stereotypical EEG features under general anesthesia while reproducing dose response characteristics for loss of consciousness. Linking loss and gain of information access to anesthesia induction and emergence, the model provides a fundamental theory of information emerging from a stochastic process, suggesting that cognitive features are enabled as a phase transition.

We consider a layered hierarchical fractal structure ascending from an input node to multiple output nodes. The layered configuration abstracts laminar and divergent organization in mammalian thalamocortical structures [20-22] (see Figure S1 in Supplemental Materials [url], which includes Refs. [23,24]). We created layers by scale-invariant fractal expansion and generated small-world properties among nodes within each layer using the Watts-Strogatz algorithm [25]. Scale-invariance and small-world organization of brain networks have been well justified [26-31]. Edges are directional ( $w_{ij} \neq w_{ji}$ ) to reflect the counter-stream architecture of the human brain [32]. Importantly, we distinguish anterior from posterior nodes by assigning different edge weights in the feedforward and feedback directions.

Let  $A_i(t)$  and  $P_j(t)$  denote neural activity of node  $i$  and preceding input from node  $j$  at time  $t$ , respectively.  $A_i(t)$  is the weighted average of activities from all input nodes:

$$A_i(t) = \frac{\sum_j w_{ij} P_j(t)}{\sum_j w_{ij}} = \frac{w_{ii} P_i(t) + \sum_{j \neq i} w_{ij} P_j(t)}{w_{ii} + \sum_{j \neq i} w_{ij}} \quad [1]$$

where  $w_{ij}$  is the weight of a directional edge from nodes  $j$  to  $i$ , and the input function  $P_j(t)$  represents the accumulated history of neural activity from preceding  $m$  time steps, weighted by exponentially decaying memory:

$$P_j(t) = \frac{\sum_{\tau=1}^m e^{-\tau} A_j(t-\tau)}{\sum_{\tau=1}^m e^{-\tau}} \quad [2]$$

We used percolation theory [33] to stochastically assign weights  $w_{ij}$  to edges using a sampling function with probability  $p$  representing likelihood of activity transmission:

$$w_{ij} = \begin{cases} \text{cdf}(U[0,1]) & i \neq j \\ ce^{-\lambda \sum_{k \neq i} w_{ki}} & i = j \end{cases} \quad [3]$$

where  $cdf$  is the Gaussian cumulative distribution function centered at  $1 - p$  with a standard deviation of 0.05 (Figure S2),  $U[0,1]$  is a uniform 0-1 distribution, and  $c$  and  $\lambda$  are constants. As  $p$  is lowered, the probability of activity transmission along individual edges is reduced, representing inhibition of information flow under anesthesia. Although different anesthetic classes act differently at molecular and cellular levels, with some potentiating inhibitory neurotransmission and others inhibiting excitatory neurotransmission, the net effect can be abstracted as a global inhibition of arousal [34]. For  $i \neq j$ , the sampling process of  $w_{ij}$  is independently varied by  $p$ . For  $i = j$ ,  $w_{ii}$  is the memory of the past activity of the same node and is influenced by the incoming connection strength. Self-connection dominates when all non-self connections diminish (*i.e.*, when  $\sum_{k \neq i} w_{ki} \rightarrow 0$ ). Since neuronal transmission, including axonal propagation and synaptic events, involves cycles of receptor inactivation, activation, and deactivation or desensitization, we account for this dynamic behavior by periodically resampling edge weights using the sampling process above. The resampling periodicity is proportional to  $e^{-\alpha p}$ , where  $\alpha$  is a constant.

We first validated the theory against previous experimental EEG studies under general anesthesia, using several clinically observed features as evaluation criteria. Four key features are hallmarks of global EEG responses: (1) characteristic EEG waveforms, including burst suppression under deep anesthesia [35], (2) EEG power shift to lower frequencies with increasing anesthetic concentrations [36], (3) synchronization of cortical nodes [37], and (4) shift of  $\alpha$  and  $\delta$  power to anterior, termed anteriorization [38]. Our model reproduces all of these clinical features simultaneously. Methods are detailed in Supplemental Materials.

Typical time-domain signals on a randomly selected output node are depicted in Figure 1a. Two different fractalizations yielded similar dependence on  $p$ . The waveforms strikingly resemble clinical EEG under different anesthesia depths [39]. As  $p$  is lowered, the dominant output frequency decreases while the amplitude increases as revealed by the spectral density in Fourier analyses (Figure 1b). Contrary to the simplistic picture of decreasing information flow during diminishing network connectivity, power rises significantly at  $p = 0.7$  in the  $\beta$  (12-30 Hz),  $\alpha$  (8-12 Hz),  $\theta$  (4-8 Hz), and  $\delta$  ( $< 4$  Hz) ranges. When a critical portion of edges is cut ( $p \approx 0.5-0.3$ ), the spectral density rapidly concentrates into  $\delta$ . At very low  $p$  values, network output exhibits bursting  $\delta$  waves (Figure 1c), resembling burst suppression under deep anesthesia. When  $p$  approaches 0, the output flatlines, corresponding to isoelectric activity of a completely

inhibited brain. These results agree with clinical observations of EEG power shift from the  $\gamma$  and  $\beta$  bands to the  $\alpha$  and  $\delta$  bands during anesthesia [36].

The model reveals that the underlying mechanism of burst suppression is edge resampling due to receptor desensitization and reactivation in a dynamic network. A decreasing  $p$  reduces the probability for signals to percolate to cortex, leading to prolonged quiescence periods. However, when edge weights are dynamically refreshed, even at very low  $p$ , some signals transiently percolate through stochastically connected edges to reach the output layers, appearing as short bursts between long suppressions.

The model also reveals that frequency shift is an emergent phenomenon, occurring precipitously in a specific range of edge probabilities. The rapid power shift to lower frequencies matches clinical EEG at a critical anesthetic concentration where consciousness is sharply and completely lost. Remarkably, this clinical feature is reproduced in random networks without a high graph density, suggesting that loss of consciousness is not localized to a specific set of neurons or receptor types but is due to large-scale, distributed action on network connectivity. Importantly, this phenomenon is input invariant and intrinsic to the dynamic process of edge connectivity.

Synchronization of output with input occurs in the same frequency ranges when power concentrates to  $\beta$ ,  $\alpha$ , and  $\delta$  bands. Figure 2a displays input-posterior output synchronization. An identical pattern was observed between input and anterior output. When  $p$  is lowered to 0.5-0.7, cortical and thalamic nodes are strongly correlated in the  $\beta$ ,  $\alpha$ , and  $\delta$  frequencies. As  $p$  is further lowered to 0.3-0.5, thalamocortical coupling exhibits a narrow band of strong synchronization in  $\gamma$  (30-75 Hz) and  $\beta$  (16-30 Hz) bands. The appearance of this strong thalamocortical synchrony at  $p \sim 0.3$  indicates information integration, whereby chaotic signals at  $p < 0.3$  become ordered and recognizable in the output. The  $\gamma$  activity in a severely inhibited network is similar to near-death EEG activity [40]. Corticocortical synchronization was also observed among output nodes. Agreeing with clinical observations under deep anesthesia [37,41,42], corticocortical synchronization in a heavily cut network occurs predominantly in the  $\delta$  and  $\theta$  frequency ranges (Figure 2b).

EEG anteriorization during anesthesia reflects asymmetric network activity. To understand its underlying mechanism, we investigated various conditions that could support asymmetric distribution of spectral power when  $p$  was reduced. We observed anteriorization only when feedback weights were greater than feedforward weights. Figure 3 displays Fourier

transformations of neural activity in the outer-most layer of a 4-degree-5-layer fractal network. Anteriorization is evident in the  $\alpha$  and  $\delta$  frequencies when the feedback:feedforward ratio is 10:1. Anteriorization co-occurs with frequency downshift and thalamocortical synchronization, signifying a shared mechanism of the same statistical process. Altering ascending projection probabilities to anterior or posterior nodes failed to produce anteriorization, suggesting that anteriorization results from inhibition of corticocortical rather than thalamocortical communications. Literature on comparative density of feedback projections in the visual system supports this finding [3,32,43,44]. Although counter-intuitive, the result underscores fundamental differences between steady-state and dynamic networks, in which response to change dominates output. As edges are incrementally cut, a network with denser (greater weight) feedback projections has disproportionately higher probability to lose feedback information flow. Our model suggests that shifts of low-frequency power to the network anterior results from exaggerated disruption in the feedback direction. This result offers an alternative interpretation for the preferential inhibition of feedback connectivity during general anesthesia [45], which occurs due to a higher baseline density of feedback connectivity under unanesthetized conditions.

Our model makes no *a priori* assumptions about molecular, cellular, or metabolic mechanisms of the network, nor does it specify constraints on connections within layers, ensuring the system's universality and scalability. By conceptualizing global arousal as stochastic edge percolation among brain centers, our model is necessarily coarse-grained without considering drug-specific and receptor-specific properties. Yet, the success of such a simple statistical model in producing multiple salient EEG features under anesthesia suggests that it simulates information transmission at a fundamental level and provides theoretical confidence in its predictive power.

A prediction of general interest is when and how cognitive features, such as sensory access, arise in an artificial network. We use the criticality of a chaos-order state transition as a surrogate measure to define the accessibility of information-encoding dynamics of a given node at other nodes. We determined conditions under which information is statistically preserved by analyzing divergence of the time-domain signal distributions when the output at a randomly selected node is used to represent the input. We quantified percolation loss as an increase in bit-wise information entropy measured by Kullback-Leibler (KL) divergence, or  $KL(P||Q)$ , where  $P$  and  $Q$  are probability distributions of input and output, respectively [46]. An order parameter is

defined as detailed in Supplemental Materials. Figure 4 shows how order emerges sharply as the network's edge probability increases from 0 to 1. Information entropy (Figure 4a) drops precipitously at  $p \approx 0.3$ . The dichotomous dependence of KL divergence on  $p$  for encoded information content is plotted in Figure 4b. A clear phase transition – with more pronounced fluctuations – occurs around  $p \approx 0.3$ . To illustrate this transition graphically, we percolated a time series encoding the pixel intensities of an 8-bit gray-scale image through the network under different  $p$  values and examined the threshold at which the integrity of the image was “recognizable” in the output layer. We calculated  $KL(P||Q) - KL_c$  for 256 different intensities (= 8 bits of information) with systematically varied  $p$  values. Each output pixel intensity was determined stochastically from  $2^{[KL(P||Q)-KL_c]}$  random values between 0 and 256 (*i.e.*,  $KL(P||Q) - KL_c$  bits of information) including the correct pixel intensity in the input image. Figure 4c shows a series of images decoded randomly at any node in the output layer at different percolation probabilities. A discernible image emerges sharply between  $p = 0.30$  and  $0.32$ . Recall that thalamocortical synchronization emerges in the  $\gamma$  and  $\beta$  band at the same  $p$  range (Figure 2a).

The sharp emergence of order with a precipitous drop in entropy approximates the steep dose-response curve for transitions between brain states during general anesthesia. More remarkably, no network connection is deterministic because weight re-assignments stochastically switch any given edge between open and closed. Moreover, graph density in our network is relatively sparse, suggesting that dense connectivity is not required to support high-level information features. That the integrity of the input image in Figure 4 is partially maintained and recognizable at  $p \approx 0.3$  suggests a low information emergence threshold. Indeed, the probability for information percolating from input to any output node at  $p \approx 0.3$  is  $<0.0081$  for the shortest path, yet inhibition at this level is robustly tolerated. The underlying process for burst suppressions, discussed above, likely contributes to the network's ability to integrate information at low  $p$ . This implies that information access can occur in simple systems as long as some type of pacemaking activity exists to coordinate dynamic recalibration of connection strength among network components. In mammalian brains, pacemakers are known to exist [47-49] and their neurobiological description is consistent with this notion.

Our model is built to provide a global view of rules governing information percolations through scalable brain connectivity, without considering many biological details. For example, we do not differentiate network inhibition through potentiation of inhibitory neurons or inhibition of excitatory neurons. Similarly, regional heterogeneities due to different populations

of receptor subtypes are not considered. Although adding more realism will likely provide more quantitative power to explain specific experimental observations, these details will not invalidate the general conclusions on the global scale, as evidenced by the model's qualitative robustness in reproducing clinical EEG features with only a single parameter.

This model has important theoretical implications, supporting the notion that consciousness may arise from the same basic statistical processes as those governing the criticality for self-organization emergence, independent of biological details [50]. Although the brain is many orders of magnitude more complex, it is tempting to speculate that transition between conscious and unconscious states is also regulated by a single connectivity parameter, especially considering the clinical observation that a sharp transition between conscious and unconscious states occurs within an extremely narrow anesthetic concentration range, with little variation among human subjects or even among different species of vastly different brain scales and capacities.

Experimentalists may test this model by measuring organized synchronous activity in brain networks, such as between primary visual cortex and frontal eye fields. A critical anesthetic dose might be identified where synchronous firing for visual attention is abruptly disrupted upon loss of consciousness. It is also possible to design a double transgenic system [51] with two reporters driven by activity-dependent immediate early genes. Comparison of co-localization of the reporters should reveal a fixed subset of neurons in conscious learning and relearning but an increasingly chaotic, non-overlapping subset of neurons in unconscious learning under varying anesthesia depths. Our model also raises the possibility of statistically improbable brain states, in which deeply inhibited neural centers become sufficiently connected through stochastic processes to support consciousness markers. Clinically, this may suggest the possibility of information incorporation in minimally conscious brains. Recent experiments in rodents have demonstrated such possibilities [19].

## **Acknowledgement**

This work was supported by grants from the National Institutes of Health (R37GM049202 and R01GM066358) and IEEE Computational Intelligence Society.

## Figure Legends

**Figure 1. Information percolation in neural network.** (a) Output activities are plotted for various  $p$  on a randomly selected node in a 1-to-4 fractalization network. Input amplitude was scaled to  $p = 1$ . Output reproduces several clinical EEG properties. At  $p = 0.2$ , burst suppression is observed. (b) Fourier analysis, averaged from 40 replicas on randomly-selected output nodes, reveals frequency shift upon network inhibition. Around  $p = 0.7$ , frequency shifts from  $\beta$  to  $\alpha$  range. Power concentrates toward  $\alpha$  and  $\delta$  ranges with decreasing  $p$ . (c) Burst suppressions become evident at low  $p$ . Corresponding time-domain activities are superimposed onto spectrograms depicting frequency components of the bursts. Without losing generality, 50% random noises were added to a 115-Hz sinusoidal signal as input.

**Figure 2. Thalamocortical and corticocortical coherence.** (a) Thalamocortical coherence, measured as cross-spectral density averaged from 40 replicas on randomly-selected posterior nodes, is plotted as a function of  $p$ . Patterns for anterior nodes are similar. Until  $p \approx 0.8$ , no coherent activity is dominant at any frequency. With further inhibition, thalamocortical coherence appears in the  $\beta$ -range and lowers to the  $\alpha$ -range at  $p \approx 0.6$ . Between  $p \approx 0.5$ -0.3, a band of  $\gamma$  coherence is visible. (b) Corticocortical coherence between two randomly-selected nodes in the output layer appears in the  $\alpha$  and  $\delta$  ranges for  $p < 0.6$ . Coherence frequencies further decrease with  $p$ . To maximize test stringency, simulations were performed using random noise as input.

**Figure 3. Anteriorization of cortical activity.** Fourier analyses of output node activity for the indicated edge probabilities. Output nodes are arranged 1 to 256 in groups of 16 from posterior to anterior. Higher power in  $\alpha$  and  $\delta$  bands shifts to the anterior (higher number) nodes with decreasing  $p$  until  $p = 0.3$ , when anteriorization effects dissipate.

**Figure 4. Emergence of correlative signal cohesion.** (a) Output information entropy, measured by the KL divergence ( $KL(P||Q) - KL_c$ ) as an order parameter, is plotted as a function of  $p$ . Each value represents bits lost in the output from 8 bits of maximum information. A phase transition is revealed at  $p \approx 0.3$ . (b) KL divergence plotted as a function of pixel intensity for  $p = 0$  (pink), 0.15 (red), 0.20 (orange), 0.25 (yellow), 0.30 (black), 0.35 (green), 0.40 (cyan), 0.45 (blue), and 1 (dark blue). Similar to (a), a clear dichotomy in information entropy occurs around  $p$  of 0.3.

Information content is lost more rapidly from high-intensity signals. (c) Graphic illustration of transitions revealed in (a) and (b): Reconstructions of an 8-bit gray-scale image at  $p = 0.00, 0.30, 0.32, 0.34, 0.38,$  and  $1.00,$  respectively. The original image features emerge sharply, becoming recognizable between  $p$  of  $0.32-0.34.$

## References

- [1] R. D. S. Raizada, *Cerebral Cortex* **13**, 100 (2003).
- [2] J. A. Hirsch and L. M. Martinez, *Current opinion in neurobiology* **16**, 377 (2006).
- [3] N. T. Markov *et al.*, *Cereb Cortex* **24**, 17 (2014).
- [4] S. L. Bressler and V. Menon, *Trends Cogn Sci* **14**, 277 (2010).
- [5] V. Menon, *Trends Cogn Sci* **15**, 483 (2011).
- [6] H. J. Park and K. Friston, *Science* **342**, 1238411 (2013).
- [7] M. L. Steyn-Ross, D. A. Steyn-Ross, J. W. Sleigh, and L. C. Wilcocks, *Phys Rev E Stat Nonlin Soft Matter Phys* **64**, 011917 (2001).
- [8] D. A. Steyn-Ross, M. L. Steyn-Ross, L. C. Wilcocks, and J. W. Sleigh, *Phys Rev E Stat Nonlin Soft Matter Phys* **64**, 011918 (2001).
- [9] M. L. Steyn-Ross, D. A. Steyn-Ross, J. W. Sleigh, and D. T. Liley, *Phys Rev E Stat Phys Plasmas Fluids Relat Interdiscip Topics* **60**, 7299 (1999).
- [10] K. Wang, M. L. Steyn-Ross, D. A. Steyn-Ross, M. T. Wilson, and J. W. Sleigh, *Front Syst Neurosci* **8**, 215 (2014).
- [11] S. N. Ching, A. Cimenser, P. L. Purdon, E. N. Brown, and N. J. Kopell, *Proceedings of the National Academy of Sciences* **107**, 22665 (2010).
- [12] S. N. Ching, P. L. Purdon, S. Vijayan, N. J. Kopell, and E. N. Brown, *Proceedings of the National Academy of Sciences* **109**, 3095 (2012).
- [13] T. Iwai, H. Kihara, K. Imaiand, and M. Uchida, *British Journal of Anaesthesia* **77**, 517 (1996).
- [14] J. H. Sheeba, A. Stefanovska, and P. V. E. McClintock, *arXiv.org q-bio.NC*, 2722 (2008).
- [15] M. M. Boly *et al.*, *Journal of Neuroscience* **32**, 7082 (2012).
- [16] I. Bojak and D. T. Liley, *Phys Rev E Stat Nonlin Soft Matter Phys* **71**, 041902 (2005).
- [17] G. Tononi, *The Biological bulletin* **215**, 216 (2008).
- [18] A. G. Casali *et al.*, *Sci Transl Med* **5**, 198ra105 (2013).
- [19] A. R. Samuelsson, N. R. Brandon, P. Tang, and Y. Xu, *Anesthesiology* **120**, 890 (2014).
- [20] S. M. Sherman, *Curr Opin Neurobiol* **22**, 575 (2012).
- [21] N. Yamamoto, *Neurosci Res* **42**, 167 (2002).
- [22] M. Inan and M. C. Crair, *Neuroscientist* **13**, 49 (2007).

- [23] T. Fedele, H. J. Scheer, G. Waterstraat, B. Telenczuk, M. Burghoff, and G. Curio, *Clin Neurophysiol* **123**, 2370 (2012).
- [24] H. J. Scheer, T. Fedele, G. Curio, and M. Burghoff, *Physiol Meas* **32**, N73 (2011).
- [25] D. J. Watts and S. H. Strogatz, *Nature* **393**, 440 (1998).
- [26] F. Aboitiz and J. F. Montiel, *Prog Brain Res* **195**, 3 (2012).
- [27] N. Kadmon Harpaz, T. Flash, and I. Dinstein, *Neuron* **81**, 452 (2014).
- [28] G. Werner, *Front Physiol* **1**, 15 (2010).
- [29] C. T. Kello, G. D. Brown, I. C. R. Ferrer, J. G. Holden, K. Linkenkaer-Hansen, T. Rhodes, and G. C. Van Orden, *Trends Cogn Sci* **14**, 223 (2010).
- [30] C. J. Stam and E. C. van Straaten, *Clin Neurophysiol* **123**, 1067 (2012).
- [31] O. Sporns, D. R. Chialvo, M. Kaiser, and C. C. Hilgetag, *Trends Cogn Sci* **8**, 418 (2004).
- [32] N. T. Markov, M. Ercsey-Ravasz, D. C. Van Essen, K. Knoblauch, Z. Toroczkai, and H. Kennedy, *Science* **342**, 1238406 (2013).
- [33] B. Bollobas and O. Riordan, *Percolation* (Cambridge University Press, 2006).
- [34] E. N. Brown, P. L. Purdon, and C. J. Van Dort, *Annual review of neuroscience* **34**, 601 (2011).
- [35] K. M. Hartikainen, M. Rorarius, J. J. Peräkylä, P. J. Laippala, and V. Jääntti, *Anesthesia and analgesia* **81**, 1223 (1995).
- [36] V. A. Feshchenko, R. A. Veselis, and R. A. Reinsel, *Neuropsychobiology* **50**, 257 (2004).
- [37] G. G. Supp, M. Siegel, J. F. Hipp, and A. K. Engel, *Current Biology* **21**, 6 (2011).
- [38] J. H. Tinker, F. W. Sharbrough, and J. D. Michenfelder, *Anesthesiology* **46**, 252 (1977).
- [39] D. L. Clark and B. S. Rosner, *Anesthesiology* **38**, 564 (1973).
- [40] J. Borjigin *et al.*, *Proc Natl Acad Sci U S A* **110**, 14432 (2013).
- [41] M. Steriade, D. Contreras, F. Amzica, and I. Timofeev, *J Neurosci* **16**, 2788 (1996).
- [42] D. Contreras and M. Steriade, *Neuroscience* **76**, 11 (1997).
- [43] J. Vezoli, A. Falchier, B. Jouve, K. Knoblauch, M. Young, and H. Kennedy, *Neuroscientist* **10**, 476 (2004).
- [44] D. J. Felleman and D. C. Van Essen, *Cereb Cortex* **1**, 1 (1991).
- [45] U. Lee, S. Kim, G. J. Noh, B. M. Choi, E. Hwang, and G. A. Mashour, *Conscious Cogn* **18**, 1069 (2009).
- [46] S. Kullback and R. A. Leibler, *Annals of Mathematical Statistics* **22**, 79 (1951).
- [47] P. Fuentealba and M. Steriade, *Progress in neurobiology* **75**, 125 (2005).

- [48] J. R. Huguenard, *Journal of Sleep Research* **7**, 24 (1998).
- [49] D. Jaeger and H. Kita, *Neuroscience* **198**, 44 (2011).
- [50] D. Krotov, J. O. Dubuis, T. Gregor, and W. Bialek, *Proc Natl Acad Sci U S A* **111**, 3683 (2014).
- [51] N. Matsuo, *Cell Rep* **11**, 351 (2015).

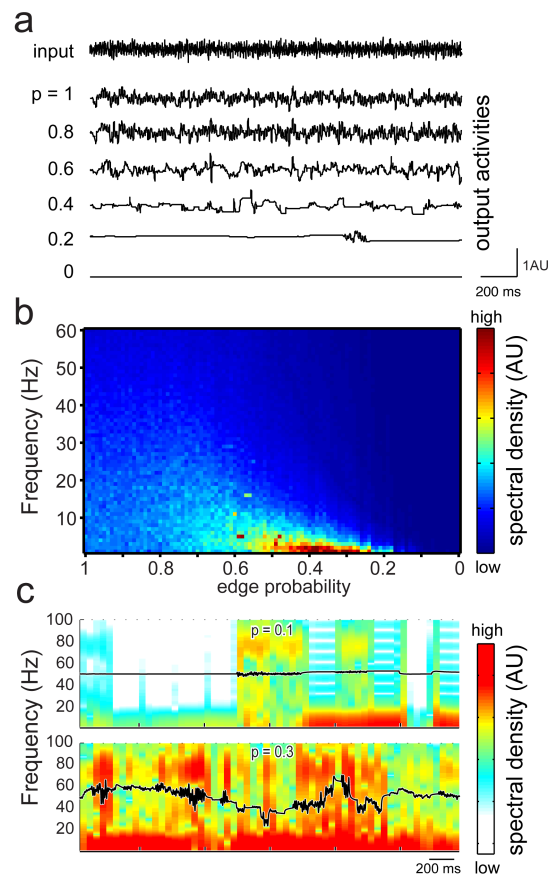


Figure 1 LB15147 29JUL2015

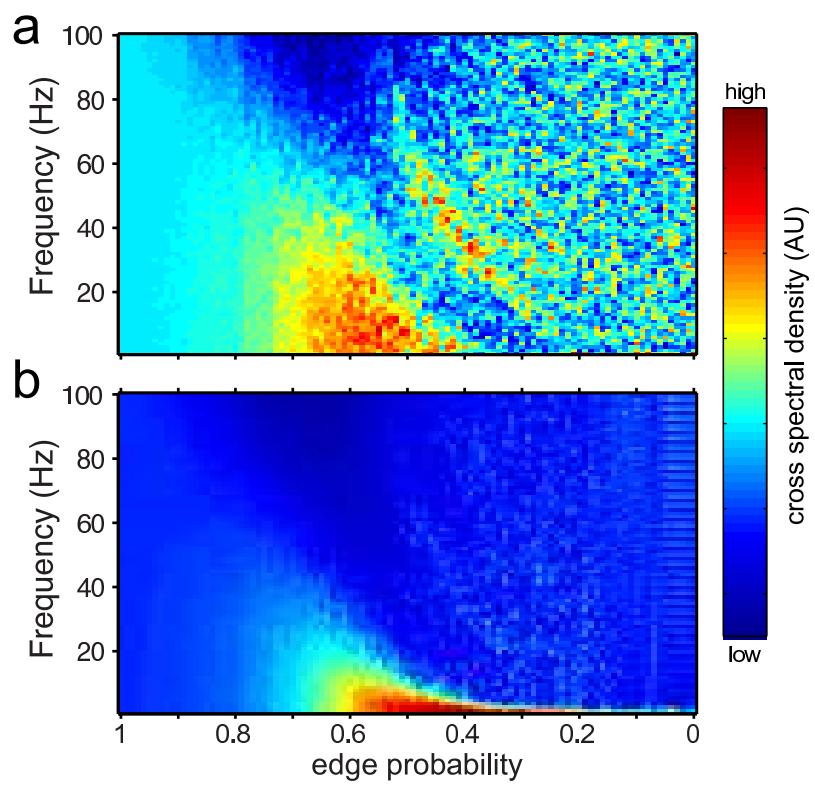


Figure 2

LB15147

29JUL2015

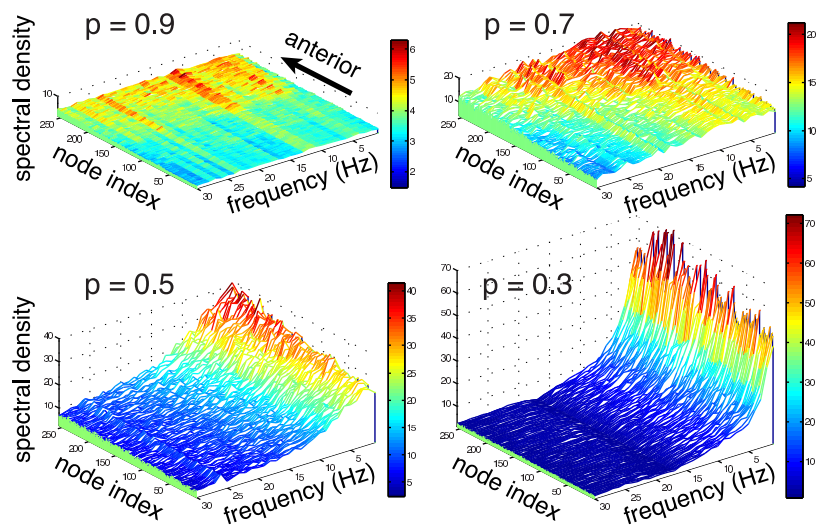


Figure 3

LB15147

29JUL2015

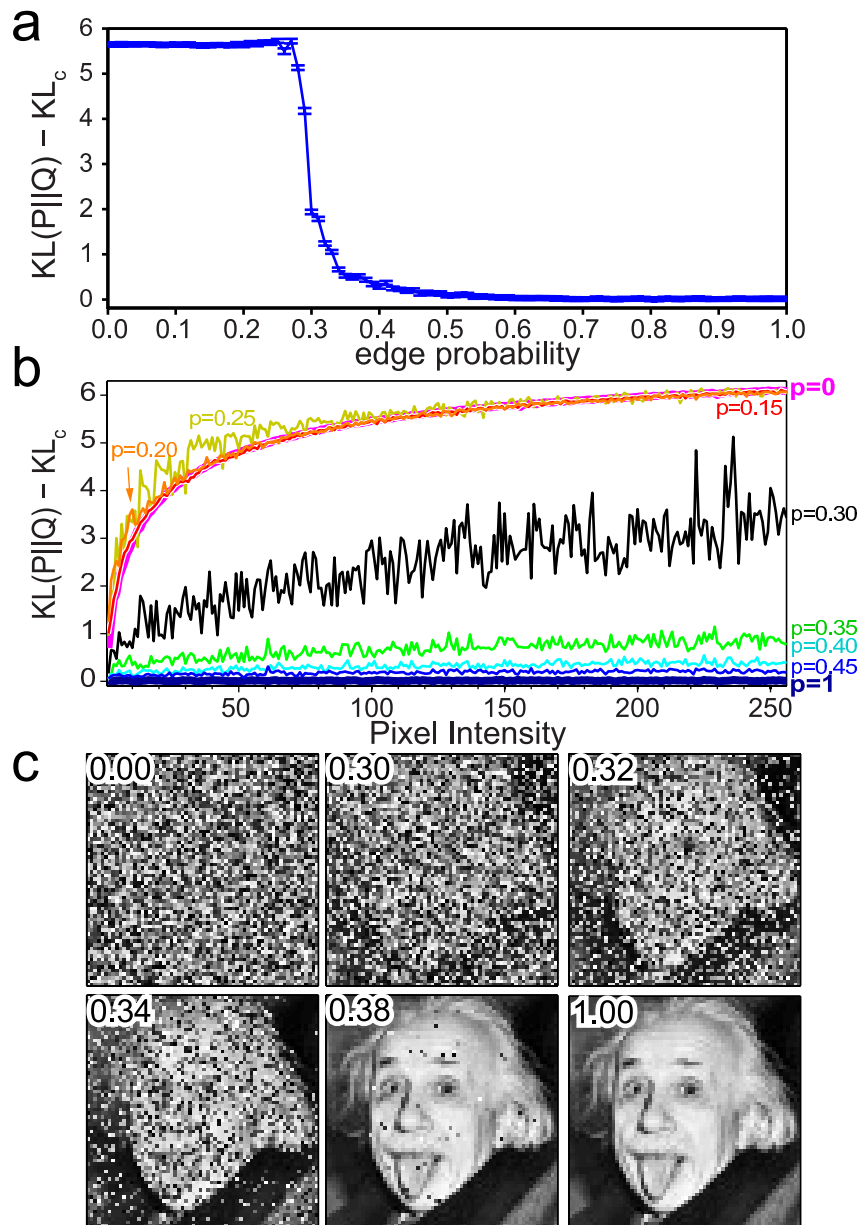


Figure 4 LB15147 29JUL2015